Charge delocalization, oxidation states and silver mobility in the mixed silver-copper oxide $AgCuO_2$[¤]

Abel Carreras,[¶] *Sergio Conejeros,*[&] *Agustín Camón,*[⊥] *Alberto García,*[#] *Nieves Casañ-Pastor,*[#,*] *Pere Alemany,*[$,*] *Enric Canadell*[#,*]

[¶] *Donostia International Physics Center, Paseo Manuel de Lardizábal, 4, 20018 Donostia-San Sebastián (Guipuzkoa), Spain*

[&] *Departamento de Química, Universidad Católica del Norte, Av. Angamos 0610, Antofagasta 124000, Chile*

[⊥] *Instituto de Ciencia de Materiales de Zaragoza-CSIC, Universidad de Zaragoza, Pedro Cerbuna 12, E-50009 Zaragoza, Spain*

[#] *Institut de Ciència de Materials de Barcelona (ICMAB-CSIC), Campus de la UAB, 08193, Bellaterra, Spain*

[$] *Departament de Ciència de Materials i Química Física and Institut de Química Teòrica i Computacional (IQTCUB), Universitat de Barcelona, Martí i Franquès 1, Barcelona 08028, Spain*

corresponding authors: Pere Alemany (p.alemany@ub.edu), Nieves Casañ-Pastor (nieves@icmab.es), Enric Canadell (canadell@icmab.es)

[¤] Dedicated to Professor Jean-François Halet on the occasion of his 60th birthday.

ABSTRACT

The electronic structure of $AgCuO_2$, and more specifically the possible charge delocalization and its implications for the transport properties, has been the object of debate. Here the problem is faced by means of first-principles density functional theory calculations of the electron and phonon band structures as well as molecular dynamics simulations for different temperatures. It is found that both Cu and Ag exhibit non-integer oxidation states, in agreement with previous spectroscopic studies. The robust CuO_2 chains impose a relatively short contact distance to the silver atoms which are forced to partially use their d_{z^2} orbitals to build a band. This band is partially emptied through overlap with a band of the CuO_2 chain which should be empty if copper were in a Cu^{3+} oxidation state. In that way, although structural correlations could roughly be consistent with an $Ag^{+}Cu^{3+}O_2$ formulation, the appropriate oxidation states for the silver and copper atoms become $Ag^{(1+\delta)+}$ and $Cu^{(3-\delta)+}$, and as a consequence, the stoichiometric material should be metallic. The study of the electronic structure suggests that Ag atoms form relatively stable chains which can easily slide despite the linear coordination with oxygen atoms of the CuO_2 chains. Phonon dispersion calculations and molecular dynamics simulations confirm the stability of the structure although pointing out that sliding of the silver chains is an easy motion that does not lead to substantial modifications of the electronic structure around the Fermi level and thus, should not alter the good conductivity of the system. However, this sliding of the silver atoms from the equilibrium position explains the observed large thermal factors.

I. INTRODUCTION

Silver-copper mixed oxides emerged as a possible alternative for high-T_c Hg-Cu superconductors because of the structural and chemical similarities between Hg^{2+} and Ag^{+}. Even if no superconducting phase of this type has so far been reported, these mixed oxides have been shown to exhibit intriguing structural and chemical properties. The first synthesized silver-copper mixed oxide was $Ag_2Cu_2O_3$,[1,2] which through chemical[3] or electrochemical[4] oxidation led to $Ag_2Cu_2O_4$ (or equivalently $AgCuO_2$), a solid of this family which has been the object of debate and presents unique features. $AgCuO_2$ was independently prepared through alternative procedures, from a $Cu(NO_3)_2$ and $AgNO_3$ solution after oxidation with persulfate,[5,6] or from electrochemical oxidation of the single metals or oxides.[4] Although the structural studies showed that the solid generated by the two procedures is essentially the same, some features led to different interpretations of the experimental findings (for instance the possibility of disorder in some sites, diamagnetism vs. weak Pauli paramagnetism, etc.) and a controversy followed concerning the electronic description of the system. Other members of this new family include $AgCu_{0.5}Mn_{0.5}O_2$,[7] $Rb_3Ag_{0.5}Cu_{0.5}O_2$,[8] $AgCu_3V_4O_{12}$[9] and $Ag_2Cu_3Cr_2O_8(OH)_4$.[10]

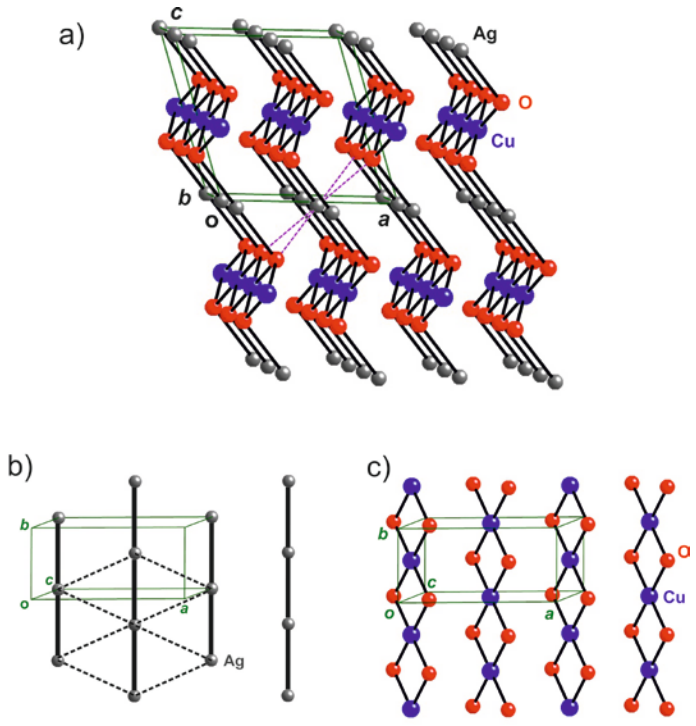

Figure 1. (a) Crystal structure of $AgCuO_2$. The long Ag···O bonds (see text) are shown as dashed purple lines. The two sublattices in $AgCuO_2$: Ag (b) and CuO_2 (c).

$AgCuO_2$ exhibits a crednerite-type structure (*C2/m*) with alternating $[CuO_2]_\infty$ and $[Ag]_\infty$ layers parallel to the *ab* planes of the crystal which are connected through Ag-O bonds (see Figure 1a). [4,6] Jansen and coworkers[6] noted that diamagnetic AgO contains two different Ag sites exhibiting linear and square planar coordinations.[11,12] Since such coordination environments are usually associated with the oxidation states, M^+ and M^{3+}, the silver atoms in AgO, formally in the Ag^{2+} oxidation state, can be considered as originating from a disproportionation process leading to Ag^+ and Ag^{3+}. By analogy they proposed that the Ag and Cu sites in $AgCuO_2$ should be associated with Ag^+ and Cu^{3+}. However, X-ray photoemission (XPS) studies[13] suggested that the situation could be more complex. For instance, in contrast with $Ag_2Cu_2O_3$, where oxidation states are unambiguously Ag^+ and Cu^{2+}, and each peak of the Ag $3d_{3/2}$ and Ag $3d_{5/2}$ doublet exhibits a single component with binding energies typical of Ag^+, the Ag 3d lines in $AgCuO_2$ present a main component and a shoulder suggesting the occurrence of both Ag^+ and Ag^{3+}. The Cu 2p region of the XPS spectra of $Ag_2Cu_2O_3$ and $AgCuO_2$ were however very similar suggesting the presence of Cu^{2+} in both cases. Thus, the $Ag^+Ag^{3+}Cu^{2+}{}_2O_4$ formulation, with mixed valence for silver, and copper in a lower oxidation state, was proposed. Subsequent XPS and X-ray absorption (XAS) measurements[14] on $AgCuO_2$ and the Ag_2O, AgO, CuO and NaCuO oxides as well as the $Ag_2Cu_2O_3$ precursor, suggested an even more complex electronic description for $AgCuO_2$, where both metal atoms are partially oxidized and the charge is delocalized among all atoms, including oxygen. As a consequence, it was suggested that the more appropriate formulation for this oxide was $Ag^{(1+x)+}Cu^{(2+y)+}O^{(2-z)-}{}_2$ with *x*, *y* and *z* values varying for the compounds generated using different synthetic procedures. This formulation was interpreted as reflecting the incipient formation of a not fully occupied Ag 4*d* band which should be associated with a good conductivity. Several observations such as a dark black color, absence of diamagnetism and a small Pauli paramagnetism were in line with this proposal.[15,16] Unfortunately, no clear-cut proof could be obtained because of the difficulty in preparing dense pellets, as the presence of silver hampers any sintering. Yet single crystal transport measurements for $Ag_2Cu_2O_3$[2] and $AgCuO_2$[15,16] made clear that the latter has conductivity values several orders of magnitude higher than the former, something that must be associated with a considerable larger electron delocalization in $AgCuO_2$.

As a matter of fact a certain ambiguity concerning the electronic nature of $AgCuO_2$ is already noticeable from a careful look at the crystal structure. The silver atoms seem to be linearly coordinated because of the two short Ag-O bonds of 2.25 Å. However there are also

four unexpectedly short 2.74 Å Ag-O contacts (see the purple dashed lines in Figure 1a) which are of the same order as the first-nearest-neighbors Ag-Ag contacts, 2.80 Å. The second set of Ag-O contacts has been found in both crystallographic and spectroscopic XAS measurements.[14] Note that the two short contacts are substantially longer than expected for a Ag(I)-O; for instance such distance is 2.07 Å in $Ag_2Cu_2O_3$.[1,2] Consequently, the Ag atoms should be better described as being in a deformed 2+4 octahedral environment, a situation certainly suggesting an oxidation state larger than +1. However, the four Cu-O distances in $AgCuO_2$ (1.83 Å) are clearly shorter than in the precursor $Ag_2Cu_2O_3$ (1.91 and 1.99 Å) making clear that copper has been oxidized; in fact the 1.83 Å Cu-O bonds are typical of Cu^{3+} (for instance they are of 1.84 Å in $NaCuO_2$ where there is no ambiguity in the oxidation state). This seems to be at odds with the previous remarks suggesting an oxidation state larger than +1 for the silver atoms. In order to check the possible occurrence of some disorder and its effect on the oxidation states, neutron diffraction experiments at 1.5 K and room temperature were carried out.[17]The Rietveld refinement showed the same atomic positions described from X-ray diffraction data at both temperatures evidencing the absence of a thermally activated disorder. The Ag thermal parameters were found to be significant at room temperature and decrease in magnitude as expected under cooling without structural change.

It must be concluded that neither the structural information coming from X-ray or neutron diffraction nor the structural analysis of the first coordination shell provided by X-ray spectroscopies lead to a complete description of the oxidation states of the copper and silver atoms in $AgCuO_2$. A recent report of *in situ* measurements of the transport properties of $AgCuO_2$ single crystals,[18] even if not allowing a conclusive statement about the conductivity regime, certainly confirms the high conductivity of the system. This observation apparently invalidates an $Ag^{+}Cu^{3+}O_2$ description of the system and can only be understood if a significant delocalization occurs, as suggested by the spectroscopic investigations. It should be mentioned that recent spectroscopic studies[18,19] have made clear that different processes at the surface of the samples (electron beam damage, partial reduction processes with formation of Ag^{o} and CuO_x-like structures during transport measurements, etc) may complicate the analysis of these measurements. In addition, difficulties in the identification of Cu^{3+} in the Cu 2*p* spectra are well-known.[19] Under such circumstances it seems that a first-principles theoretical study of the stoichiometric solid could provide important clues to rationalize the electronic description of this material. Thus, in the present work we examine the situation from the viewpoint of first-principles density functional theory (DFT) calculations. We analyze in detail the band structure and phonon spectrum of stoichiometric $AgCuO_2$ and carry

out a molecular dynamics study at different temperatures to explore the stability of the structure. New specific heat measurements and previously reported neutron diffraction data for $AgCuO_2$[17] usefully complement the discussion.

II. COMPUTATIONAL DETAILS AND EXPERIMENTAL MEASUREMENTS

Calculations to explore the electronic structure of $AgCuO_2$ have been carried out with a numeric atomic orbitals density functional theory (DFT) approach[20] implemented in the SIESTA code.[21] We tested the performance of three generalized gradient approximation (GGA)-type functionals: Perdew-Burke-Ernzerhof (PBE),[22] revised PBE (PBEsol),[23] and Wu-Cohen (WC)[24] in describing the crystal structure of the system. For reasons detailed below all results reported here have been obtained with the PBEsol functional. For all elements we have used a split-valence double-ζ basis set including polarization functions (DZP).[25] The core electrons have been replaced by norm-conserving scalar relativistic pseudopotentials[26] factorized in the Kleinman-Bylander form.[27] The density matrix elements have been converged to a threshold between cycles of 10^{-4}. The mesh cutoff parameter for the real space integration is set to 350 Ry and the electronic smearing temperature to 5 meV. For the calculations of the band structure and the Fermi surface we used a *k*-point mesh with 4220 *k*-points generated by a diagonal (20×20×20) matrix using a Monkhorst-Pack scheme.[28] For calculations of the energy profiles under several distortions we have used a reduced set of 172 *k*-points generated by a diagonal (7×7×7) matrix and 63 *k*-points generated by a diagonal (5×5×5) matrix in calculations for a (2×2×1) supercell.

The Vienna *ab initio* simulation (VASP) code[29] was used for calculation of the phonon spectrum and molecular dynamics trajectories at 11 different temperatures between 100 K and 600 K in the NVT ensemble using the Nosé-Hoover thermostat.[30,31] The lattice parameters have been determined by relaxing the crystal structure using the PBEsol[23] functional and the core electrons were treated by means of the projector augmented wave method.[32,33] Geometry relaxation and phonon calculations used a plane wave basis set with an energy cut-off of 300 eV, a gaussian smearing with sigma of 0.05, the conventional unit cell with 8 atoms and a (4×4×4) *k*-points mesh using a Monkhorst-Pack scheme.[28]

The MD calculations have been carried out using the PBEsol functional,[23] gaussian smearing with sigma of 0.05 and a (2×2×2) supercell with 64 atoms. The Brillouin zone was sampled with the Γ point. We used a time step of 1.0 fs and 10.000 total time steps. The

calculation of the power spectrum has been performed with the DynaPhoPy program[34] using the last 8.000 time steps of each MD simulation.

The sorting plots based on the correlations between *d*-orbital occupation and core orbital binding energies were obtained using the *ab initio* CRYSTAL17 code[35-37] and using the B3LYP functional.[38] The all-electron atomic Gaussian basis sets used were of the 8-6-411-(41d)G and 9-7-6631(41d)G types for Cu and Ag, respectively.[39] For the calculation of the Coulomb and exchange integrals, tolerance factors of 7, 7, 7, 7, and 14 were used. The convergence criterion for the electronic energy was set at 10^{-7} a.u. The experimental crystal structures (see the Supporting information for the complete list of compounds) were used to generate these sorting plots.

$AgCuO_2$ powder for experimental measurements was obtained from electrochemical oxidation of $Ag_2Cu_2O_3$ in alkaline media in the conditions described in ref. [4]. A stirred suspension of $Ag_2Cu_2O_3$ in a 1M NaOH solution was used and the experiments were carried out in a three-electrode cell. A platinum foil (1 cm^2) was used as working electrode; platinum wires (1 mm diameter) were used as pseudo-reference electrode and counter electrode, respectively. The counter electrode was placed in a separate half-cell, connected to the other half cell by glass fritted membrane to avoid direct contact with the suspension. The experiments were controlled using a McPile II, BioLogic Science Instruments galvanostat/potentiostat.

Specific Heat measurements were performed using a Quantum Design Physical Property Measurements system after a magnet reset, from 2 to 275 K. 3 mm diameter pellets of $AgCuO_2$ compressed from powder, and weighing 0.96 mg were held to the cryostat holder using Apiezon N grease, that was measured independently and subtracted from the total signal. Xray powder diffraction after the measurement was made on a rotating anode Rigaku Rotaflex Ru-200B diffractometer with CuKα radiation (λ1 = 1.5406 Å and λ2 = 1.5444 Å) with a step size of 0.02° and using a scanning rate of 0.16°/min. No evidence of any additional phase derived from $AgCuO_2$ reduction was found.

III. RESULTS and DISCUSSION

A. Crystal structure. It will be important to fully understand the electronic description of $AgCuO_2$ to realize that its crystal structure can be *formally* assembled from two different types of chains along the *b* direction: (i) Ag chains and (ii) CuO_2 chains (see Figures 1b and 1c). In fact when discussing about Ag chains one should bear in mind that every Ag atom is

also connected axially to two O atoms of the CuO_2 chains. However, this partition of the crystal structure provides a useful starting point to understand the electronic structure. The Ag-Ag distance within the chain is 2.80 Å while successive chains are displaced by half the unit cell along *b* thus forming a pseudo-hexagonal layer of Ag atoms and the interchain Ag···Ag distance is 3.34 Å. The CuO_2 chains contain Cu in a square planar coordination with four equivalent Cu-O bonds of 1.83 Å and angles of 80º and 100º. Successive chains are also displaced half a unit cell along *b*.

Table 1. Comparison of room temperature X-ray refinement data[13] and optimized cell parameters for $AgCuO_2$.

	***a* (Å)**	***b* (Å)**	***c*(Å)**	**β (º)**	**V (Å^3)**
X-ray data	6.054	2.799	5.851	107.9	94.359
PBE	6.445	2.892	5.935	113.3	101.569
PBEsol	5.955	2.866	5.768	109.6	92.722
WC	5.910	2.865	5.771	108.7	92.538

We first tested the performance of several functional (PBE, PBEsol and WC) in coping with the main structural details of the system. Shown in Table 1 is the comparison of the experimental and calculated results for the cell constants. Both the PBEsol and WC functionals lead to results in good agreement with the experimental data, with a slight underestimation of the volume (-2%) and very similar errors for all optimized unit cell parameters, which are kept within a small range between -2% and 2%. In contrast, the PBE functional leads to a large overestimation of the volume (+8%) mostly due to a large overestimation of the *a* parameter.

Table 2. Comparison of room temperature X-ray refinement data[13] and optimized bond distances and angles for $AgCuO_2$.

	Ag⋯Ag (Å)	**Ag⋯O (Å)**	**Cu⋯O (Å)**	**O-Cu-O (º)**
X-ray data	2 × 2.80 4 × 3.34	2 × 2.25 4 × 2.74	4 × 1.83 2 × 2.70	2 × 80. 2 × 100.
PBE	2 × 2.89 4 × 3.53	2 × 2.21 4 × 2.65	4 × 1.93 2 × 3.04	2 × 83. 2 × 97.
PBEsol	2 × 2.87 4 × 3.30	2 × 2.18 4 × 2.58	4 × 1.91 2 × 2.69	2 × 83. 2 × 97.
WC	2 × 2.87 4 × 3.28	2 × 2.18 4 × 2.59	4 × 1.92 2 × 2.64	2 × 83. 2 × 97.

The most relevant bond geometrical parameters obtained in these optimizations are reported in Table 2. The noted overestimation of the *a* cell parameter when using the PBE functional leads to distances between neighboring Ag and CuO_2 chains which are strongly overestimated by this functional. The intra-chain parameters are reasonably well reproduced with any of the three functionals. Consequently only the PBEsol and WC functionals provide a well-balanced description of the intra- and inter-chain interactions in $AgCuO_2$. The results obtained with both functionals are comparable. Let us note that all details of the electronic structure obtained with the optimized geometries of these functionals and the experimental crystal structure are very similar. However since the optimized geometry is the appropriate starting point for the molecular dynamics runs, and both PBEsol and WC functionals provide very similar results, in the following we will only report those obtained with PBEsol based on the optimized structure (Table S1 in Supplementary Information).

B. Electronic structure and conductivity. Before looking in detail at the nature of bonding in this phase let us consider the question of the conductivity in the pristine stoichiometric phase. The calculated band structure of $AgCuO_2$ is reported in Figure 2a. An important observation is that two pairs of bands, with a non-negligible dispersion of around 1 eV, cross the Fermi level along several directions of the Brillouin zone thus suggesting a metallic behavior. These partially filled bands lead to the complex Fermi surface of Figure 3 containing a kind of tubular contribution along the a^*+c^* direction and a series of large and irregular closed pockets centered at the E point of the Brillouin zone. In addition there are some marginally small closed pockets. The tubular contribution is associated with electron

carriers and the closed pockets around E with hole carriers. Stoichiometric $AgCuO_2$ is thus predicted to be a three-dimensional (3D) metal.

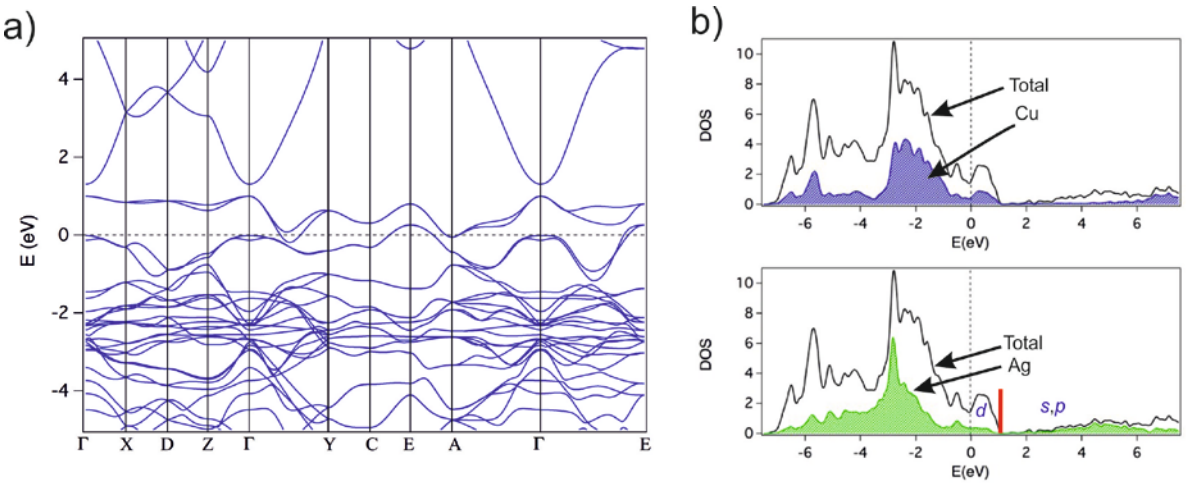

Figure 2. (a) Band structure calculated for $AgCuO_2$ using the C-centered monoclinic lattice where the energy zero is the Fermi level. Γ = (0, 0, 0), X = (0.5, 0, 0), D = (0.5, 0, 0.5), Z = (0, 0, 0.5), Y = (0, 0.5, 0), C = (0, 0.5, 0.5), E = (0.5, 0.5, 0.5) and A = (0.5, 0.5, 0) in units of the reciprocal lattice vectors. (b) Density of states (DOS) and partial contribution of the Cu and Ag orbitals for $AgCuO_2$.The red line in the bottom panel separates the regions where the Ag *d* and Ag *s* + *p* orbitals are dominant.

The origin of this metallic behavior is clear-cut when looking at the lower panel of Figure 2b, which contains the calculated density of states (DOS) for $AgCuO_2$ as well as the contribution of the Ag orbitals. The Ag levels below the red line are mostly associated with *d*-type orbitals. Since the Fermi level occurs at a lower energy it is obvious that the *d* levels of silver are not completely full and consequently, the Ag^+ oxidation state does not reflect the actual electronic structure of the system. The DOS diagrams of Figure 2b also indicate that around the Fermi level the Cu and Ag orbitals participate to a similar extent and that there is also a substantial participation of oxygen levels. Note that the Fermi surface corresponds to a 3D-type conductivity. Consequently, such conductivity cannot independently arise from the silver (i.e. AgO_2) and CuO_2 chains, which run along the *b*-direction: a non-negligible interaction between the two types of chains is needed to lead to the 3D conductivity. In summary, the present results provide support for the idea that stoichiometric $AgCuO_2$ must exhibit a substantial electronic delocalization leading to non-integral oxidation states for both Ag and Cu atoms and that irrespective of the hypothetical presence of metallic silver at the surface, the system should be conducting. As mentioned, despite difficulties in measuring the

conductivity, relatively high values have been reported for $AgCuO_2$.[15] This feature has been assumed to provide proof for the non-integer oxidation states suggested by the spectroscopic studies.[14]

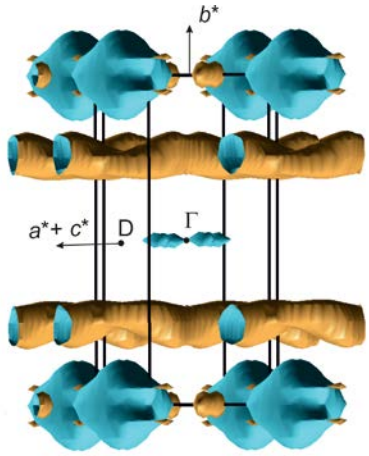

Figure 3. Calculated Fermi surface for $AgCuO_2$.

C. Electronic structure and oxidation states. Let us now consider in more detail the question of the appropriate oxidation states. From the two alternative extreme formulations, $Ag^{+}Cu^{3+}O_4$ and $Ag^{2+}Cu^{2+}O_4$, chemical wisdom tends to favor the former: Ag^{2+} is a rare oxidation state usually unstable toward disproportionation and structural data for linear coordinate silver/square planar coordinated copper are usually associated with Ag^{+}/Cu^{3+}. The Mulliken (Total)/(*d* orbital) populations calculated for $AgCuO_2$ are 10.130/9.278 for Cu and 10.204/9.606 for Ag and the total value for O is 6.833. Although these values are smaller for Cu pointing towards a larger oxidation state, the differences are certainly not that large so as to justify the $Ag^{+}Cu^{3+}O_4$ formulation. Looking for a simple but informative way to clarify this question we have pursued two different but complementary approaches: (i) developing some sorting plots correlating the oxidation states of Cu and Ag with some magnitude that can be obtained from first-principles calculations for a large series of compounds where the oxidation states are unambiguous, and (ii) analyzing in detail the electronic structure of $AgCuO_2$.

Since the calculated Mulliken atomic populations do not seem to yield large differences in electron populations for the different oxidation states, we have used an additional indicator, the energy of a selected core level, to devise a procedure yielding reasonable differences to allow a distinction of the oxidation states of Cu and Ag.[40] The basic idea is that a higher

oxidation state will lead to a lower population of the *d* shell of a given atom while core electrons will be more tightly bound in higher oxidation states. Plotting the *d* electron population vs. the binding energy of the selected core level (minus the orbital energy according to Koopman's theorem so that they should not be directly compared with experimental values) should provide a sorting plot able to separate the regions associated with different oxidation states. Since an all electron basis set is needed to calculate energy eigenvalues for core electrons we have carried out the calculations using the CRYSTAL program. Although the conclusions are practically independent of the functional used, the best results were obtained with the hybrid B3LYP functional.[38] The sorting plots developed for Ag and Cu are shown in Figures 4a and 4b, respectively.

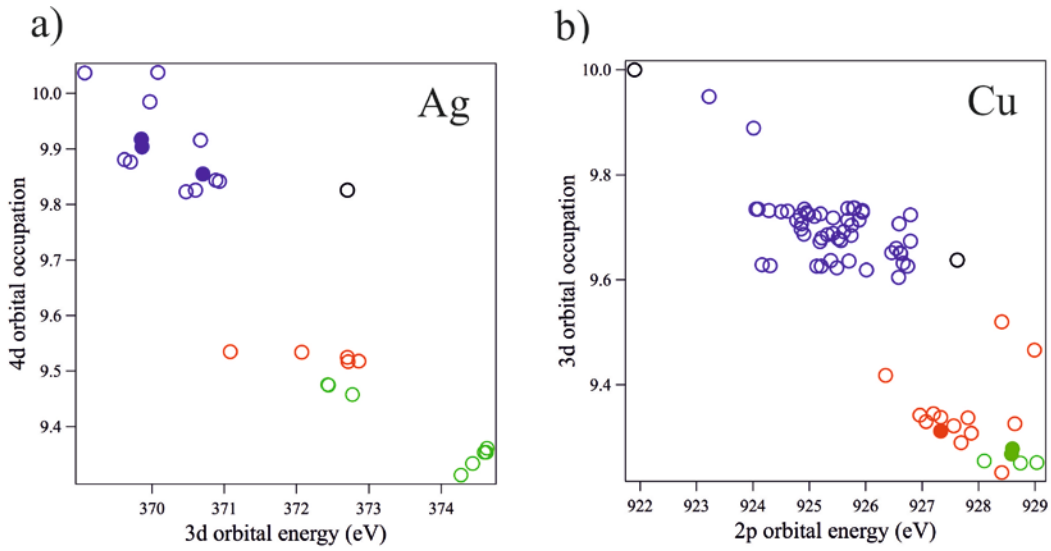

Figure 4. Sorting plots of *d* orbital occupation according to a Mulliken population analysis vs. core orbital binding energy for silver (a) and copper (b) compounds calculated using the hybrid B3LYP functional (see the Supplementary information for a full list of compounds used to generate these plots) Empty circles correspond to atoms with unambiguously defined oxidation states. Filled circles correspond to mixed silver-copper oxides. Color coding: M in black, M^{+} in blue, M^{2+} in red, and M^{3+} in green.

According to the B3LYP calculations the silver atoms in $AgCuO_2$ have a 4*d* orbital population of 9.904e- and the core 3*d* binding energy is 369.9 eV. Using the plot of Figure 4a these values clearly indicate that Ag is in an Ag^{+} oxidation state. The Cu 3*d* orbital occupation in $AgCuO_2$ is 9.278e- and the core 2*p* binding energy is 928.6 eV. These values

are perfectly compatible with a Cu^{3+} oxidation state according to the plot of Figure 4b. Although calculations for copper compounds do not allow a sharp distinction between the Cu^{2+}/Cu^{3+} oxidation states, those for silver compounds (Figure 4a) allow to definitively discard the hypothesis of an Ag^{2+} oxidation state.

We are thus led to the conclusion that the $Ag^{+}Cu^{3+}O_4$ formulation provides the best starting point to describe the electronic situation in $AgCuO_2$. This is in agreement with well-known structural trends in Cu-based high T_c superconductors[41] as well as with our discussion above, where we noted that the Cu-O distance in $AgCuO_2$ is similar to that in $NaCuO_2$. Yet, a Cu^{3+} oxidation state implies that silver is present in $AgCuO_2$ as Ag^{+}, something meaning that the Ag *d* levels are completely full. However, this is not the case as a consequence of the overlap between the Cu and Ag *d*-based bands of Figure 2 so that such formulation must be refined in order to fully describe the system. Let us revisit the electronic structure calculations of Figure 2. From very simple bonding concepts, if we consider the Cu^{3+} ions (d^8) to be in a 4+2 distorted pseudo-octahedral environment, the Cu levels in the vicinity of the Fermi level should correspond to those arising from the formally antibonding e_g* levels that are split by the 4+2 distortion, leaving the d_{z2} orbital filled and the d_{xy} orbital orbital empty (here we use a local coordinate system with the z axis perpendicular to the CuO_2 chains and the x and y axes approximately in the bisectors of the Cu-O bonds). For a formally Ag^{+} ion (d^{10}) in a linear coordination, we would expect all five *d* levels to be filled, with the d_{z2} level being the highest in energy for an orientation in which the two short Ag-O bonds are aligned with the z axis (Note that in this discussion we use two alternative orientations to define the *d* orbitals of Cu and Ag, respectively).

The detailed analysis of the different contributions to the DOS of the *d* orbitals of Cu and Ag are reported in Figures S1 and S2, respectively, of the Supplementary Information. As expected, all contributions, except those of the Cu d_{xy} and Ag d_{z2} (see Figure 5) occur below the Fermi level and thus, the associated orbitals are completely filled. The contribution of the Cu d_{xy} and Ag d_{z2} orbitals to the DOS (green and purple shaded regions, respectively in Figure 5) are quite different. The Cu d_{xy} plot is what should be expected for the present system: two well separated peaks centered at very different energies associated with the Cu-O bonding levels (around -5.8 eV) and Cu-O antibonding levels (at +0.5 eV, see also the COHP curve for the short Cu-O contacts in Figure S3) separated by a region with considerably smaller values associated with the delocalization of these levels around the solid through interactions with the silver atoms.

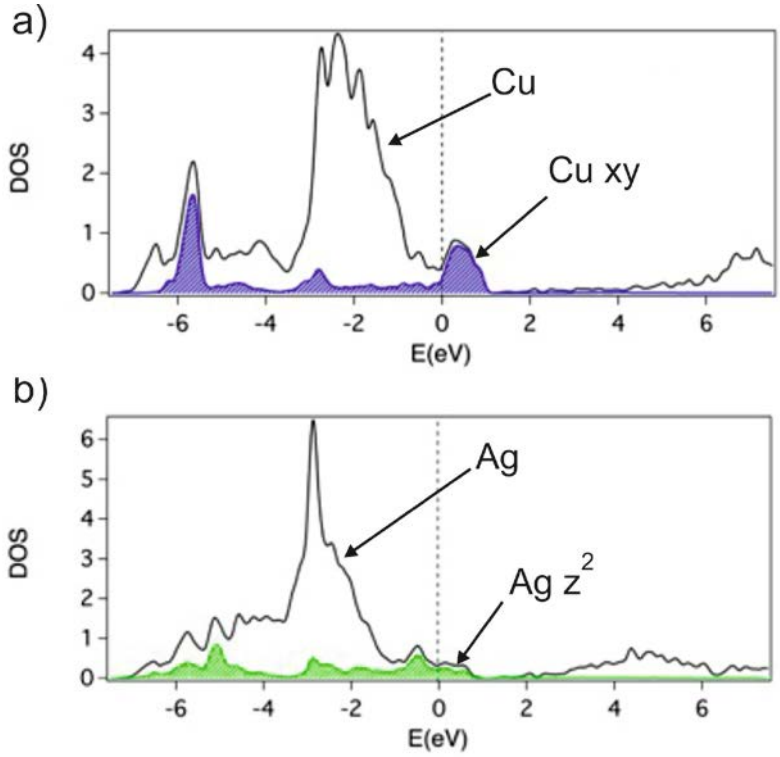

Figure 5. (a) Contribution of the Cu orbitals (black line) to the DOS of $AgCuO_2$ and partial contribution of the Cu d_{xy} (purple shaded region). (b) Contribution of the Ag orbitals (black line) to the DOS of $AgCuO_2$ and partial contribution of the Ag d_{z2} (purple shaded region). See the text for the local axes used for labeling the orbitals.

The Ag d_{z2} curve is very different. Although the two maxima corresponding to the Ag-O bonding (at -5. eV) and antibonding levels (-0.6 eV) are visible, they are not that different from many of the values in-between as it was the case for the Cu d_{xy} curve. This simply means that the Ag d_{z2} orbitals contribute not only to the localized levels associated with the Ag-O bonds but also to quite delocalized states. As can be easily seen in Figure 1a, the Ag-Ag separation is imposed by the relatively rigid CuO_2 chains since the silver atoms must be coordinated by the oxygen atoms of these chains. This leads to an intrachain Ag-Ag distance of 2.80 Å which is surprisingly short for an Ag^+-Ag^+ contact (the Ag-Ag distance in elemental silver is even larger, 2.89 Å). As a consequence, the circular ring of d_{z2} orbitals in adjacent Ag atoms along the *b* direction overlap very well and acquire dispersion leading to relatively large and spread contributions along the main peaks (i.e. the band that becomes emptied around the point E of the band structure in Figure 2a). This peculiar feature of the $AgCuO_2$ structure has two important consequences. First, the d_{z2} orbitals are only partially used to establish the Ag-O bonds and this is why, as noted above, these bonds are considerably

weaker and thus, longer than expected (2.25 Å but 2.07 Å in $Ag_2Cu_2O_3$ with a non-ambiguous Ag^+). Second, the upper part of the d_{z2} contribution which occurs above the Fermi level is empty. Since this part is that associated with the d_{z2}--d_{z2} interactions leading to the Ag-based band and the upper part of this band is antibonding, the emptying of these levels provides a substantial stabilization to the Ag sublattice which must be considered, at least partially, as a silver chain. The situation is reminiscent of the stabilization of the Pt chains in $K_2[Pt(CN)_4]Br_{0.3}\cdot 3H_2O$ (KCP) and other highly conducting one-dimensional systems[42,43] where the upper part of a transition metal based band is partially emptied because of doping, leading to the formation of the chain and the metallic character.

In summary, the stable CuO_2 chains of $AgCuO_2$ impose a relatively short contact distance to the silver atoms since they coordinate with the O atoms of the CuO_2 chains. As a result they are forced to partially use their d_{z2} orbitals to build a band dispersive along the chain (i.e. *b*) direction and in that way overlap appreciably with the Cu d_{xy} based band, so that the CuO_2 chains act effectively as a dopant of the silver chains. Consequently, as noted above the $Ag^+Cu^{3+}O_2$ formulation is a useful starting point to describe the gross structural features of this phase, but a slightly different formulation with non-integral oxidation states for both Cu and Ag, $Ag^{(1+\delta)+}Cu^{(3-\delta)+}O_2$, accounts better for the actual electronic distribution, spectroscopic observations and transport properties. Another important consequence is that the building of the partially emptied (doped) band is detrimental to the stability of the Ag-O linear bonds. Consequently it may be expected that the silver atoms of $AgCuO_2$ form silver chains which can easily slide along the *b* direction.

D. Silver mobility. The structural data for $AgCuO_2$ exhibits some unusual aspects such as weak peaks that could imply breaking of the C-centering, weak diffuse scattering lines suggesting the possible occurrence of disorder, etc.[4,13] The possibility that the presently known structure is some kind of average structure cannot be dismissed. In addition, the results of the previous section and the noted anomalous coordination of the silver atoms in the crystal structure, which in fact exhibit large thermal factors,[4,13] suggest that the silver atoms could exhibit some mobility. In order to shed some light into this question we have first calculated and analyzed the phonon structure for the optimized $AgCuO_2$ crystal structure.

The phonon dispersion diagram (Figure 6a) shows that this structure is indeed a stable structure (the very small negative frequencies found for wave vectors in the Γ-Y direction in the proximity of the center of the Brillouin zone can be attributed to small numerical errors). The phonon DOS curve (Figure 6b, left) and the phonon partial DOS (Figure 6b, right)

indicate that the low energy modes (below 8 THz) involve mainly the movement of Ag and Cu atoms, with the movement of Ag atoms being predominant in the lowest energy modes (below 3 THz). Participation of oxygen atoms in this energy region is small and it becomes predominant in the intermediate region, between 8 and 15 THz. The high energy peak around 16 THz involves the movement of both the Cu and O atoms in similar proportions. Note, however that heavier atoms, such as Ag in this case, have always a larger participation in the lower frequency modes, so that the interpretation of the participation of atoms of different mass in the DOS is not straightforward and should be taken only as a qualitative indication. Altogether, these data suggest that the present structure is dynamically stable and not susceptible to a major energy lowering distortion.

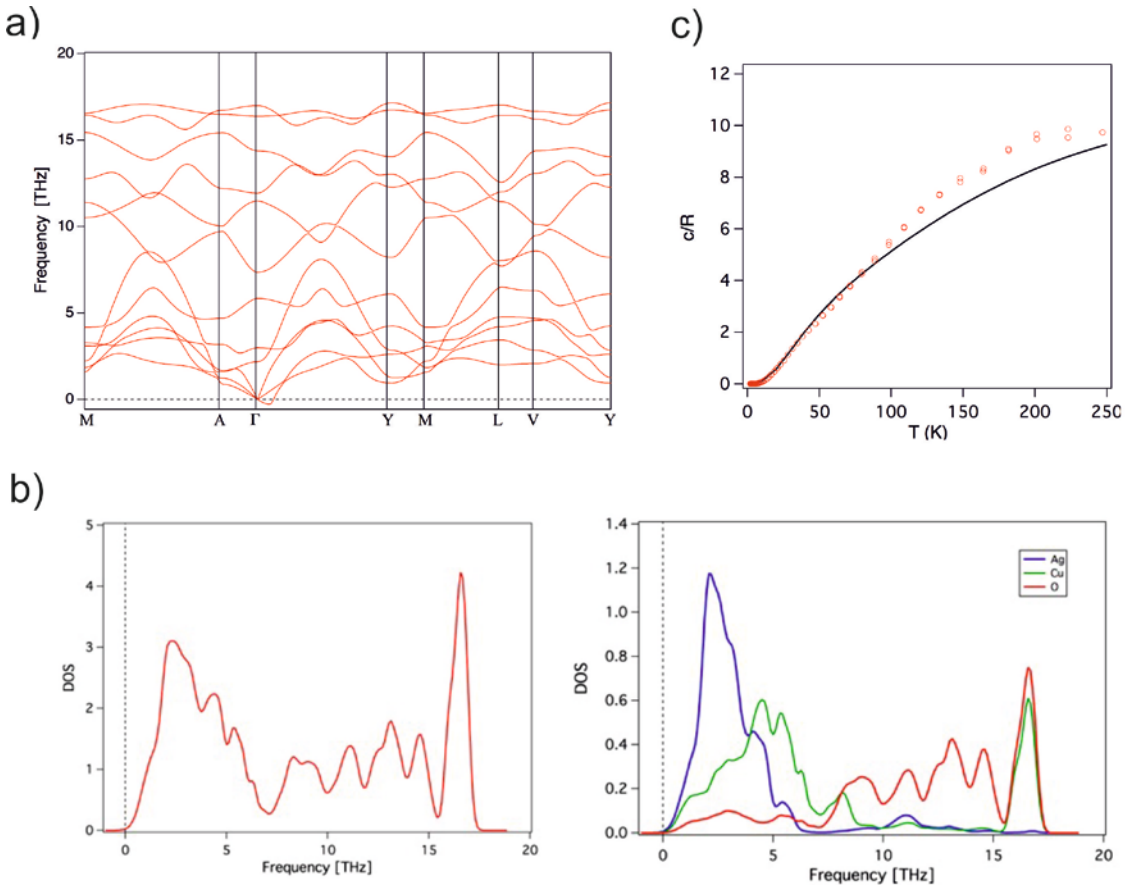

Figure 6. (a) Phonon dispersion diagram calculated for $AgCuO_2$ using the primitive monoclinic lattice (*a*'= 1/2(*a*-*b*), *b*'= 1/2(*a*+*b*), *c*'= *c*), where Γ= (0, 0, 0), V = (0.5, 0, 0), L = (0.5, 0, 0.5), A = (0, 0, 0.5), Y = (0.5, 0.5, 0.0) and M = (0.5, 0.5, 0.5) in units of the reciprocal lattice vectors. (b) Total (left) and partial (right) phonon density of states for

$AgCuO_2$. (c) Heat capacity at constant volume obtained from the calculated phonon spectrum (black curve) compared with the experimental data (red circles).

In order to confront these results with experimental data we have measured the heat capacity and calculated the heat capacity at constant volume. The results are shown in Figure 6c. With four atoms per unit cell the heat capacity should reach a limiting value of 12R at high temperatures. The calculated curve agrees very well with the experimental data at low temperatures, up to approximately 100 K, and rises a bit less steeply for larger temperatures. The experimental results show that no abrupt localization of a disordered structure is present, as it could be expected, at low temperatures. The differences at high temperatures are most likely due to the large anharmonic phonon modes in the $AgCuO_2$ structure which are not taken into account in the phonon calculation. Anharmonicity effects lead to a softening of phonon frequencies and consequently these modes will have larger contributions to the heat capacity at lower temperatures than in a model considering only harmonic vibrations. Consequently, although according to these results the present structure is stable at low temperatures we should more carefully consider the possible influence of anharmonicity effects at higher temperatures.

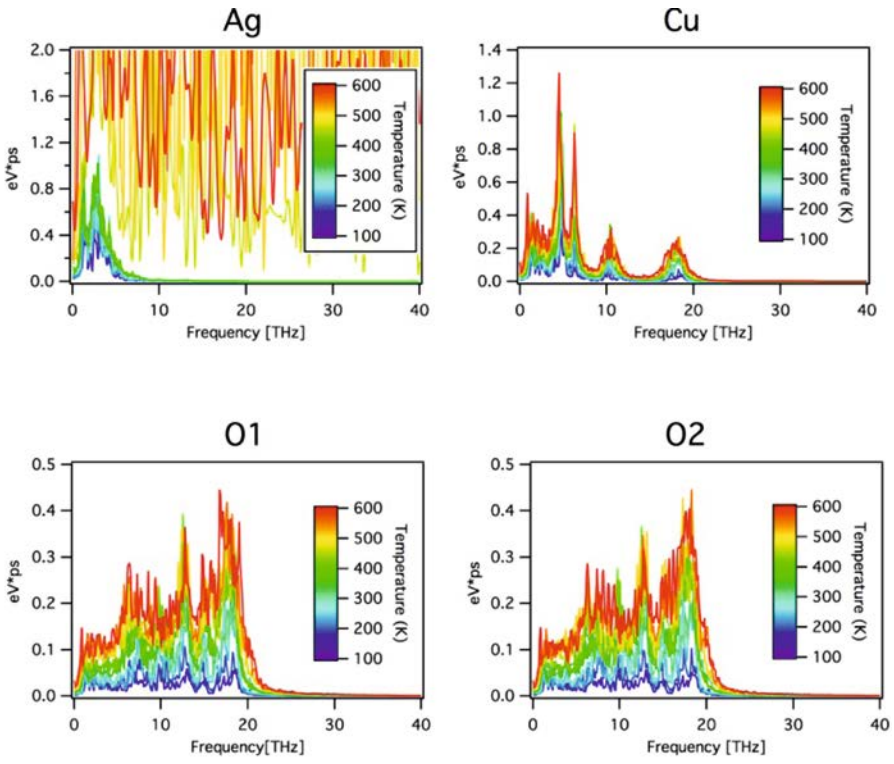

Figure 7. Power-spectrum of the mass-weighted velocity of Ag, Cu, O1, and O2 atoms of $AgCuO_2$ at several temperatures in the range 100 - 600K.

In order to further analyze the dynamic behavior of $AgCuO_2$ we have calculated the power spectrum of the mass-weighted velocity of Ag, Cu and O atoms based on molecular dynamics simulations, thus taking into account anharmonicity effects. The power spectrum has been obtained by Fourier transformation of the mass-weighted velocity autocorrelation function obtained from a molecular dynamics simulation (see computational details). We have thus carried out molecular dynamics simulations for 11 different temperatures from 100 K to 600 K. The power-spectrum indicates the presence of periodicities in the molecular dynamics trajectory (in the autocorrelation function we calculate the correlation between the velocity of an atom at a time t_0 and its velocity after some time t_0+t, and hence, if the atom is vibrating, a peak will appear in the power-spectrum at the frequency of the vibration). Those calculated for Ag, Cu and O atoms in the two independent positions at different temperatures are shown in Figure 7. In the infinite supercell limit, the sum of the power-spectrum calculated for all atoms is related to the phonon DOS within a constant factor. The peaks appearing in the power spectrum for a given atom coincide broadly with the projected densities of states in Figure 6b although there may be some discrepancies. These arise mainly from the fact that we use a finite cell in the molecular dynamics trajectory, and the fact that the phonon spectrum in Figure 6a has been obtained within the harmonic approximation while the power-spectrum obtained from a molecular dynamics trajectory takes into account the anharmonicity effects at finite temperature.

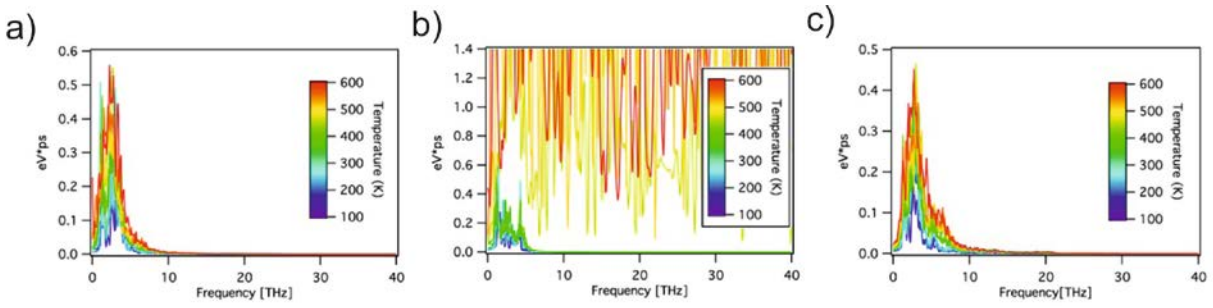

Figure 8. Power-spectrum calculated for the velocities of the Ag atoms in the x, y, and z directions at several temperatures in the range 100 - 600K. The coordinate axis is such that the x and y axes run along the *a* and *b* directions, respectively.

At low temperatures all four power-spectra in Figure 7 have a peak structure similar to the corresponding projections of the phonon DOS curves in Figure 6b. The most interesting feature appears for Ag atoms between 400 and 450 K, where the power spectrum loses its structure indicating the lack of correlation between their velocity at a given time and sometime later, or in other words, the more or less free movement of the Ag atoms within the structure at temperatures above approximately 400 K. This is an important result which can be analyzed in more detail by calculating the Ag power spectrum for each direction of space separately. The three graphs included in Figure 8 show very clearly that the lack of correlation between the motions of Ag atoms at longer times is circumscribed to the motion along the direction of the silver chains parallel to the crystallographic *b* axis (y axis in our calculation). It can thus be concluded that the motion of Ag atoms upon raising the temperature increases progressively with larger and larger vibrations around their equilibrium position until a critical temperature between 400 and 450 K is reached when the Ag chains most likely begin to freely slide in a direction parallel to the crystallographic *b* axis. Previously reported neutron diffraction experiments at 1.5 K and room temperature in reference[17] support these results. In these refinements the same structure reached from X-ray data refinement[4,13] is found, and additionally such structure is found both at room temperature and 1.5K, evidencing the absence of a thermally activated disorder. The Ag thermal parameters are significant at room temperature and decrease in magnitude, as expected, under cooling. Structural work at higher temperatures would be worthwhile doing in order to test the results of our study.

To have a better idea of the silver atoms displacements we carried out a series of model calculations using a $2a\times2b\times c$ supercell of the optimized structure thus containing four silver chains with two atoms per chain, where only the silver atoms were allowed to move. Since we are using the optimized structure with the CuO_2 sublattice kept frozen the calculated activation energies will be overestimated and should be taken as an upper bound. The sliding of undistorted silver chains was found to be the easier type of distortion. For instance, the sliding of a single chain in the $2a\times2b\times c$ supercell is associated with an activation energy of 0.25 eV. A dimerization within the silver chain is associated with an activation energy around three times larger. Distortions implicating lateral displacements of the silver atoms lead to large activation energies (around ten times that of the sliding motion). Since the 0.25 eV activation energy is an upper bound we conclude that sliding of the silver chains are easy motions which may occur at not too high temperatures. Calculations where more than a single chain are sliding suggest that the sliding of adjacent chains should be practically uncorrelated. An important result is that these sliding motions do not lead to substantial modifications of

the overlapping copper and silver based bands around the Fermi level and there is no opening of a gap at the Fermi level. Thus, the sliding motions should not alter the good conductivity of the system. However, this sliding back and forth of the equilibrium position should induce the observed large thermal factors along the *b* direction.

At this point one may wonder why the sliding motion of the silver chains is an easy process. Every silver atom is linearly coordinated to two oxygen atoms and these bonds must be partially broken during the sliding. Here we must remember that these two Ag-O bonds (2.25 Å) are substantially longer than expected because the Ag d_{z2} orbital, which is responsible for the Ag-O short bonds, is also partially used to establish the Ag-Ag interactions. In addition, there are four additional long Ag-O contacts (2.74 Å) with O atoms of adjacent CuO_2 chains completing a 2+4 distorted octahedral environment (see Figure 1a). The ratio between the calculated overlap populations, which are a measure of the bond strength, associated with the short vs. long Ag-O contacts is only 2.4 (i.e. 0.048 vs 0.020) despite the substantially different distances. However, since there are 4 long contacts but only 2 short contacts per Ag atom actually seen in the path, the total overlap population per Ag atom is almost equally shared by the two types of contacts. As a consequence, when a silver atom moves along the chain direction, the decrease in bonding due to increasing Ag···O distances for part of the Ag-O bonds is partially cancelled by the bonding increase with other oxygen atoms. The long Ag-O contacts, although seemingly negligible from a structural point of view, play thus a substantial role in understanding the mobility of the silver atoms and the overall stability of the structure.

IV. CONCLUDING REMARKS

The puzzling electronic structure of $AgCuO_2$ has been studied by means of first-principles DFT calculations as well as molecular dynamics simulations. These studies provide evidence that both Cu and Ag must be considered as having non-integer oxidation states thus supporting previous spectroscopic studies. The CuO_2 chains impose a relatively short Ag-Ag contact distance to the silver atoms which are forced to partially use their d_{z2} orbitals to build a band. This band is partially emptied through overlap with the band of the CuO_2 chain built from the Cu d_{xy} levels, which should have been empty if the appropriate oxidation state for Cu were Cu^{3+}. In that way, although structural correlations are consistent with the formulation $Ag^{+}Cu^{3+}O_2$, the appropriate oxidation states for the silver and copper atoms in $AgCuO_2$ become $Ag^{(1+\delta)+}$ and $Cu^{(3-\delta)+}$. The overlap of these silver and copper based bands is

responsible for the absence of an energy gap at the Fermi level and consequently, the stoichiometric material should exhibit metallic behavior. The analysis of the DFT band structure also suggests that the Ag atoms in $AgCuO_2$ should form relatively stable chains which, despite being linearly coordinated with oxygen atoms of the CuO_2 chains, can easily slide among the CuO_2 chains. Phonon dispersion calculations and molecular dynamics simulations confirm the stability of the structure. However, they also point out that sliding of the silver chains is an easy motion keeping the band overlap around the Fermi level and thus should not alter the good conductivity of the system. Full agreement is found with the new specific heat and previous neutron diffraction data that evidences the same structure both at room and low temperature, without abrupt phase transitions.

ACKNOWLEDGMENTS.

This work was supported by MINECO (Spain) through Grants FIS2015-64886-C5-4-P, CTQ2015-64579-C3-3-P and MAT2015-65192-R, Generalitat de Catalunya (2017SGR1506, 2017SGR1289 and XRQTC) and FONDECYT (Chile) through project 11107163. E.C., N.C-P. and A. G. acknowledge support of the Spanish MINECO through the Severo Ochoa Centers of Excellence Program under Grant SEV-2015-0496, and P. A. from the Maria de Maeztu Units of Excellence Program under Grant MDM-2017-0767. We are grateful to Dr. David Muñoz-Rojas for kindly providing the sample for heat capacity measurements and Dr. Juan Rodríguez-Carvajal for his assistance during the neutron diffraction studies mentioned in the text. We also thank the Servicio General de Apoyo a la Investigación SAI, Universidad de Zaragoza.

ASSOCIATED CONTENT

Three figures with the complete analysis of the Cu 3*d* and Ag 4*d* contributions to the density of states of $AgCuO_2$ as well as the COHP curves for the Ag-O and Cu-O contacts, PBEsol optimized structure for $AgCuO_2$, and information about the crystal structures used in generating the sorting plots in Figure 4.

AUTHOR INFORMATION

ORCID

Enric Canadell: 0000-0002-4663-5226

Pere Alemany: 0000-0002-3139-6189
Nieves Casañ-Pastor: 0000-0003-2979-4572
Alberto García: 0000-0001-5138-9579
Sergio Conejeros: 0000-0002-2490-1677
Abel Carreras: 0000-0001-5529-2440

Note

The authors declare no competing financial interest

REFERENCES

1. Gómez-Romero, P.; Tejada-Rosales, E. M.; Palacín, M. R. $Ag_2 Cu_2 O_3$: The First Silver Copper Oxide. *Angew. Chem. Int. Ed.* 1999, 38, 524-525.
2. Tejada-Rosales, E. N.; Rodríguez-Carvajal, J.; Casañ-Pastor, N.; Alemany, P.; Ruiz, E.; El-Fallah, S.; Alvarez, S.; Gómez-Rodríguez, P. Room Temperature Synthesis and Crystal, Magnetic, and Electronic Structure of the First Silver Copper Oxide. *Inorg. Chem*. **2002**, *41*, 6604-6613.
3. Muñoz-Rojas, D.; Fraxedas, J.; Gómez-Romero, P. ; Casañ-Pastor, N. Room temperature solid-state transformation from $Ag_2Cu_2O_3$ to $Ag_2Cu_2O_4$ by ozone oxidation *J. Solid State Chem*. **2005**, *178*, 295-305.
4. Muñoz-Rojas, D.; Oró, J.; Gómez-Romero, P.; Fraxedas, J.; Casañ-Pastor, N. Electrochemically induced reversible solid state transformations: electrosynthesis of $Ag_2Cu_2O_4$ by room temperature oxidation of $Ag_2Cu_2O_3$. *Electrochem. Commun*. **2002**, *4*, 684-689.
5. Curda, J. ; Klein, W. ; Jansen, M. $AgCuO_2$—Synthesis, Crystal Structure, and Structural Relationships with CuO and $Ag^{I}Ag^{III}O_2$. *J. Solid State Chem*. **2001**, *162*, 220-224.
6. Curda, J.; Klein, W.; Liu, H.; Jansen, M. Structure redetermination and high pressure behaviour of $AgCuO_2$. *J. Alloys Comp*. **2002**, *338*, 99-103.
7. Muñoz-Rojas, D.; Subías, G.; Oró-Solé, J.; Fraxedas, J.; Martínez, B.; Casas-Cabanas, M.; Canales-Vázquez, J.; González-Calbet, J.; García-González, E.; Walton, R. I.; Casañ-Pastor, N. Ag_2CuMnO_4: A new silver copper oxide with delafossite structure**.** *J. Solid State Chem*. **2006**, *179*, 3883-3892.
8. Sofin, M.; Peters, E.-M.; Jansen, M. Crystal structure of rubidium copper silver oxide, $Rb_3Cu_{0.5}Ag_{0.5}O_2$. *Z. Kristallogr. NCS* **2003**, *218*, 379-380.

9. Akizuki, Y.; Yamada, I.; Fujita, K.; Akamatsu, H.; Irifune, T.; Tanaka, K. $AgCu_3V_4O_{12}$: a Novel Perovskite Containing Mixed-Valence Silver ions. *Inorg. Chem*. **2013**, *52*, 13824-13826.

10. Casañ-Pastor, N.; Rius, J.; Vallcorba, O.; Peral, I.; Oró-Solé, J.; Cook, D. S.; Walton, R. I.; García, A.; Muñoz-Rojas, D. $Ag_2Cu_3Cr_2O_8(OH)_4$:A new bidimensional silver-copper mixed - oxyhydroxide with in-plane ferromagnetic coupling. *Dalton Transactions* **2017**, *46*, 1093-1104.

11. Jansen, M.; Fischer, P. Eine neue Darstellungsmethode für monoklines Silber(I,III)oxid (AgO), Einkristallzüchtung und Röntgenstrukturanalyse. *J. Less-Common Metals* **1988**, *137*, 123-131.

12. Yvon, K.; Bezinge, A.; Tissot, P.; Fischer, P. Structure and magnetic properties of tetragonal silver(I,III) oxide, AgO. *J. Solid State Chem*. **1986**, *65*, 225-230.

13. Muñoz-Rojas, D.; Oró, J.; Fraxedas, J.; Gómez-Romero, P.; Casañ-Pastor, N. Structural study of electrochemically-synthesized $Ag_2Cu_2O_4$. A novel oxide sensitive to irradiation. *Cryst. Eng*. **2002**, *5*, 459-467.

14. Muñoz-Rojas, D.; Subías, G.; Fraxedas, J.; Gómez-Romero, P.; Casañ-Pastor, N. Electronic Structure of $Ag_2Cu_2O_4$. Evidence of Oxidized Silver and Copper and Internal Charge Delocalization. *J. Phys. Chem. B* **2005**, *109*, 6193-6203.

15. Sauvage, F.; Muñoz-Rojas, D.; Poeppelmeier, K. R. ; Casañ-Pastor, N. Transport properties and lithium insertion study in the p-type semi-conductors $AgCuO_2$ and $AgCu_{0.5}Mn_{0.5}O_2$. *J. Solid State Chem*. **2009**, *182*, 374-380.

16. Muñoz-Rojas, D.; Córdoba, R.; Fernández-Pacheco, A.; De Teresa, J. M.; Sauthier, G.; Fraxedas, J.; Walton, R. I. ; Casañ-Pastor, N. High Conductivity in Hydrothermally Grown $AgCuO_2$ Single Crystals Verified Using Focused-Ion-Beam-Deposited Nanocontacts. *Inorg. Chem.* **2010**, *49*, 10977-10983.

17 David Muñoz Rojas, PhD thesis, Universitat Autònoma de Barcelona, 2004 (https://www.tdx.cat/handle/10803/3184).

18. Tchaplyguine, M.; Zhang, Ch.; Andersson, T.; Björneholm, O. Ag–Cu oxide nanoparticles with high oxidation states: towards new high T_c materials. *Dalton Trans*. **2018**, *47*, 16660-16667.

19. Svintsitskiy, D. A.; Kardash, T. Yu.; Boronin, A. I. Surface dynamics of mixed silver-copper oxide $AgCuO_2$ during X-ray photoelectron spectroscopy study. *Appl. Surf. Sci*. **2019**, *463*, 300-309.

20. (a) Hohenberg, P.; Kohn, W. Inhomogeneous Electron Gas. *Phys. Rev.* **1964**, *136*, B864–B871. (b) Kohn, W.; Sham, L. J. Self-Consistent Equations Including Exchange and Correlation Effects. *Phys. Rev.* **1965**, *140*, A1133–A1138.
21. (a) Soler, J. M.; Artacho, E.; Gale, J. D.; García, A.; Junquera, J.; Ordejón, P.; Sánchez-Portal, D. The Siesta method for ab initio order-N materials simulation. *J. Phys.: Condens. Matter*. **2002**, *14*, 2745–2779; (b) Artacho, E.; Anglada, E.; Diéguez, O.; Gale, J. D.; García, A.; Junquera, J.; Martin, R. M.; Ordejón, P.; Pruneda, J. M.; Sánchez-Portal, D.; Soler, J. M. The Siesta method: developments and applicability. *J. of Phys.: Condens. Matter* **2008**, *20*, 064208.
22. Perdew, J. P.; Burke, K.; Ernzerhof, M. Generalized Gradient Approximation Made Simple. *Phys. Rev. Lett*. **1996**, *77*, 3865–3868.
23. Perdew, J. P.; Ruzsinszky, A.; Csonka, G. I.; Vydrov, O. A.; Scuseria, G. E.; Constantin, L. A.; Zhou, X.; Burke, K. Restoring the Density-Gradient Expansion for Exchange in Solids and Surfaces. *Phys. Rev. Lett*. **2008**, *100*, 136406.
24. Wu, Z.; Cohen, R. E. More accurate generalized gradient approximation for solids. *Phys. Rev. B* **2006**, *73*, 235116.
25. Artacho, E.; Sánchez-Portal, D.; Ordejón, P.; García, A.; Soler, J. M. Linear-Scaling ab-initio Calculations for Large and Complex Systems. *Phys. Stat. Sol. (b)* **1999**, *215*, 809–817.
26. Troullier, N.; Martins, J. L. Efficient Pseudopotentials for plane-wave calculations. *Phys. Rev. B* **1991**, *43*, 1993–2006.
27. Kleinman, L.; Bylander, D. M. Efficacious Form for Model Pseudopotentials. *Phys. Rev. Lett*. **1982**, *48*, 1425–1428.
28. Monkhorst, H. J.; Pack, J. D. Special points for Brillouin zone integrations. *Phys. Rev. B* **1976**, *13*, 5188–5192.
29. Kresse, G.; Furthmüller, J. Efficient iterative schemes for *ab initio* total-energy calculations using a plane-wave basis set. *Phys. Rev. B* **1996,** *54* 11169–86.
30. Nosé, S. A unified formulation of the constant temperature molecular dynamics methods**.** *J. Chem. Phys.* **1984**, *81*, 511-519.
31. Hoover, W. G. Canonical dynamics: Equilibrium phase-space distributions. *Phys. Rev. A* **1985**, *31*, 1695-1697.
32. Blöchl, P. E. Projector augmented-wave method. *Phys. Rev. B* **1994**, *50*, 17953-17979.
33. Kresse, G.; Joubert, D. From ultrasoft pseudopotentials to the projector augmented-wave method. *Phys. Rev. B* 1999, *59* 1758-1775.

34. Carreras, A.; Togo, A.; Tanaka, I. DynaPhoPy: A code for extracting phonon quasiparticles from molecular dynamics simulations. *Comp. Phys. Comm*. **2017**, *221*, 221-234.
35. Dovesi, R.; Erba, A.; Orlando, R.; Zicovich-Wilson, C. M.; Civalleri, B.; Maschio, L.; Rerat, M.; Casassa, S.; Baima, J.; Salustro, S.; Kirtman, B. Quantum-mechanical condensed matter simulations with CRYSTAL. WIREs *Comput. Mol. Sci*. **2018**, *8*, e1360.
36. See http://www.crystal.unito.it for Details on the CRYSTAL Code, Gaussian BasisSets, Computational Schemes, etc.
37. Dovesi, R.; Saunders, V. R.; Roetti, C.; Orlando, R.; Zicovich-Wilson, C. M.; Pascale, F.; Civalleri, B.; Doll, K.; Harrison, N. M.; Bush, I. J.; DArco, P.; Llunell, M.; Caus, M.; Nol, Y.; Maschio, L.; Erba, A.; Rerat, M.; Casassa, S. CRYSTAL17, (2017) CRYSTAL17 User's Manual. University of Torino, Torino.
38. Becke, A. D. Density-functional thermochemistry. III. The role of exact exchange. *J. Chem. Phys*., **1993**, *98*, 5648.
39. Dall'Olio, S.; Dovesi, R.; Resta, R. Spontaneous polarization as a Berry phase of the Hartree-Fock wave function: The case of $KNbO_3$. *Phys. Rev. B* **1997**, *56*, 10105.
40 Sergio Conejeros Espínola, PhD thesis, Universitat de Barcelona, 2013 (http://hdl.handle.net/10803/131399).
41. Rao, C. N. R.; Ganguly, A. K. Structural aspects of superconducting cuprates. *Acta Cryst. B* **1995**, *51*, 604-618.
42. Whangbo, W.-H.; Hoffmann, R. The band structure of the tetracyanoplatinate chain. *J. Am. Chem. Soc*. **1978**, *100*, 6093-6098.
43. Canadell, E.: Doublet, M.-L.: Iung, C. *Orbital Approach to the Electronic Structure of Solids,* Oxford University Press, Oxford, UK (2012), chapter 8.

Table of Contents Entry

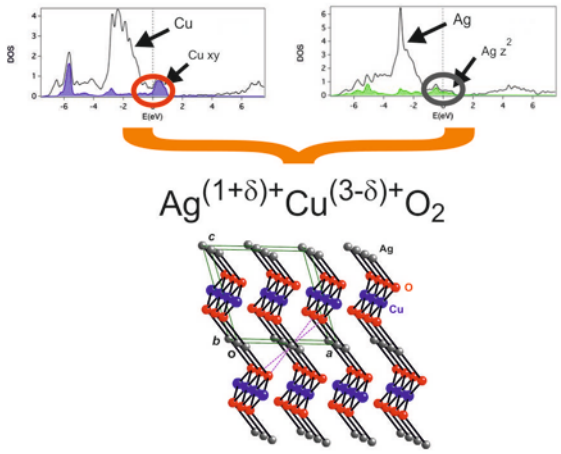

Because of the overlap between Cu and Ag *d*-based bands $AgCuO_2$ must exhibit metallic conductivity and the transition metal atoms hold non-integer oxidation states. Phonon dispersion calculations and molecular dynamics simulations confirm the stability of the structure although pointing out that sliding of the silver chains should be an easy motion.